Electronic Journal of Structural Engineering

Original Article

Cite this: DOI:10.56748/ejse.25756

Received Date: 20 January 2025
Accepted Date: 3 June 2025

1443-9255
https://ejsei.com/ejse

Spilt Tensile Strength of Fiber-Reinforced Recycled Aggregate Concrete Simulation Employing Tunned Random Forests Trees

Xiao Chen [a#], Chen Xi [a*#], Min Xiao [a], Lang Wu [a]

[a] School of Civil Engineering, Jiangxi Science and Technology Normal University, Nanchang, Jiangxi,330013, China
* Corresponding authors: XiChen202407@126.com
[#] Joint first authors

Abstract

A significant quantity of waste concrete is produced each year due to the demand for concrete manufacturing, which drives the yearly need for raw materials. Recycled aggregate concrete has become a viable remedy as a result. It is vulnerable to breaking and has less strength since the hardened mortar is affixed to natural aggregates, which presents a problem. The goal of this research is to employ random forests (RF) frameworks to project the split tensile strength (STS) of fiber-reinforced recycled aggregate concrete (RAC). The RF framework uses the Chimp optimization algorithm (CHOA) and artificial hummingbird optimization (ARHA) to tweak hyperparameters and select the best-performing combination. A data set including 257 data points and 10 input variables was taken from peer-reviewed published research and arbitrarily split into three phases: training, validating, and testing. The RF-AR approach exhibited high reliability, with R^2 of 0.9942, 0.9824, and 0.9913 throughout the training, validating, and testing stages. RF-AR had higher results than RF-CH, with R^2 of 0.9796, 0.9566, and 0.9694, respectively. Considering the values of the Theil Inequality Coefficient (TIC), RF-AR depicted the lowest values at 0.0128, 0.0213, and 0.0171 concerning 0.0241, 0.0333, and 0.0318 related to RF-CH throughout the training, validating, and testing stages. All in all, the RF-AR strategy performed better, even if the RF-CH method was dependable in forecasting the STS of fiber-reinforced RAC.

Keywords

Recycled aggregate concrete, Fiber reinforced concrete, Spilt tensile strength, Random forests, Sensitivity analysis

1. Introduction

From 1928 to 2018, cement production generated roughly 38 billion tons of greenhouse gas emissions worldwide. A substantial 71% of this huge amount was produced post-1990. In 2019, worldwide cement output totaled 4.1 billion tons (Kuijpers, 2020). The use of reclaimed concrete waste as a replacement for certain coarse aggregates in the production of recycled aggregate concrete (RAC) has become a modern practice in the concrete industry (Hassankhani & Esmaeili-Falak, 2024; Moradi et al., 2022; Zarei et al., 2024). The cost of using recycled aggregate into concrete is generally cheaper than utilizing new resources. *RAC* significantly reduces the volume of waste sent to landfills and minimizes the energy and carbon emissions associated with the production of novel substances.

In the manufacturing process, the reclaimed aggregate consistently comprises both conventional aggregate and hardened mortar. As a result, the strength of the recovered aggregate is inferior to that of conventional aggregate, principally due to the intrinsic weakness of the hardened mortar and the interfaces between the mortar and conventional aggregate. Furthermore, the crushing process results in the development of many fissures within the reclaimed aggregate (Babak et al., 2024; Fonseca et al., 2011; Younis & Pilakoutas, 2013). The constraint substantially impedes its prospective applications. Therefore, the cracking characteristics of reclaimed aggregate concrete should be prioritized over its other mechanical properties.

The inclusion of different fibers enhances the crack resistance of fiber-reinforced recycled aggregate concrete (*RAC*) (Benemaran et al., 2024; Chakradhara Rao et al., 2011; Katkhuda & Shatarat, 2017; Meesala, 2019). Akca et al. (Akça et al., 2015) conducted a study where polypropylene fibers were used to reinforce *RAC*, and it was demonstrated that both the flexural strength and splitting tensile strength increased as the fiber content increased. In a separate study, Ali et al. (B. Ali & Qureshi, 2019) compared the mechanical attributes of glass fiber-reinforced *RAC* with plain *RAC*, and a noticeable improvement was observed in the splitting tensional resistance of fiber-reinforced *RAC*. In their research, Gao et al. (Gao & Zhang, 2018) conducted a study on the function of steel fiber-reinforced *RAC*. They observed a significant improvement in the flexural strength as the volume fraction of steel fibers increased. This research concludes that the use of fibers significantly improves the crack resistance of *RAC*. It is crucial to acknowledge that multiple actors affect the reinforcing mechanism such as fiber type, fiber geometry (length and aspect ratio), volume percentage, interfacial bonding between fibers and matrix, and fiber dispersion within the matrix.

Various approaches have been suggested to forecast the cracking behavior of plain concrete, including bending tests, analytical methods, and mechanical models (Afkhami Hoor & Esmaeili-Falak, 2024; Y. Chen et al., 2022; Hu et al., 2022; Sun et al., 2019; Yuan et al., 2020). These strategies seek to improve the accuracy of predictions by analyzing several aspects. Nonetheless, precisely characterizing the cracking properties of concrete remains difficult. These methods aim to enhance forecasting reliability by examining influential parameters such as tensile strength, fracture energy, modulus of elasticity, aggregate type and size, water-to-cement ratio, and the microstructure of the cementitious matrix.

Machine learning methods have emerged as novel approaches for tackling various estimating challenges in civil and structural engineering, such as predicting crack propagation, compression and tensile properties, modulus of elasticity, durability under environmental stressors, and load-bearing capability of concrete components (Bayrami, 2021; Dawei et al., 2023; Esmaeili-Falak et al., 2019; Esmaeili-Falak & Benemaran, 2023, 2024; Esmaeili-Falak & Sarkhani Benemaran, 2024; Li et al., 2023; Liang & Bayrami, 2023; Mohammadi Yaychi & Esmaeili-Falak, 2024s). In their research, investigators endeavored to employ machine learning (ML) to forecast the cracking conduct of RAC (Amin et al., 2022; Neshatfar & Sekeh, 2024; Pan et al., 2022). They effectively created several ML models that demonstrated outstanding performance. It is important to highlight that throughout the development of these *ML* models, the fundamental physical interpretation was overlooked, and the influence of fibers was not considered (Kumarawadu et al., 2024).

Previous research focused mostly on the essential elements utilized in the concrete manufacturing process. Furthermore, studies on reinforced concrete with recycled aggregates do not account for the influence of fibers. The assessment of cracking patterns in recycled aggregate concrete (*RAC*) gets increasingly complex when accounting for the influence of recycled aggregates (*RA*), together with the further complications presented by fiber reinforcement in *RAC*. Given the paucity of research on the split tensile strength of fiber reinforced recycled aggregate concrete, it is imperative to undertake a comprehensive study to design, validate, and evaluate algorithms for forecasting split tensile strength. This study develops machine learning techniques for the structural performance of fiber-reinforced recycled aggregate concrete. The robust RF framework is considered for this purpose. The *RF* the framework uses the Chimp optimization algorithm (CHOA) and artificial hummingbird optimization (*ARHA*) for hyperparameter tweaking and selecting the greatest performing combination of hyperparameters (M. A. S. Ali et al., 2022; Alnaggar et al., 2022; Bagherabad et al., 2025; Neshatfar et al., 2023; Umba et al., 2024). A data set including 257 data points and 10 input variables was taken from peer-reviewed published research and arbitrarily split into three phases: testing, validating, and training. The effectiveness of every approach was evaluated using a variety of metrics. Additionally, the new sensitivity analysis method assesses each parameter's effect on the goal. The primary contribution of this work is to assess the fundamental principles of several machine learning approaches and to evaluate their performance in forecasting the STS of RAC. Additionally, using several machines to learn algorithms makes it easier for academics to evaluate and contrast their results using the same dataset.

2. Dataset Pre-Evaluation

In solid materials, an indirect tensile test is commonly employed to investigate their cracking behavior, with the indirect tensile resistance acting as strength to cracking. As a result, the indirect tensile resistance of Recycled Aggregate Concrete (RAC) is designated as the target variable for assessing crack evaluation. At the same time, different influential agents are considered input parameters and a collection of statistically and physically pertinent input features such as mixture composition, aggregate features, fiber content and kind, and mechanical properties are included as separate variables in the modeling process. These two sets of parameters are the basis for constructing machine learning databases. The initial phase of machine learning entails the critical selection of variables and data collection, which directly influences the accuracy and practicality of soft computing approaches. Conventional soft computing approaches often fail to consider the physical significance of parameters, leading to constrained simulations and the inability to handle scenarios beyond the existing dataset. Hence, physical tests and established mechanical approaches are utilized to assist in developing the database. Following the established norms for attribute selection, a combined sum of 257 data entries was gathered from the available literature sources (B. Ali & Qureshi, 2019; Andreu & Miren, 2014; Butler et al., 2013; Chakradhara Rao et al., 2011; S. Chen et al., 2022; Das et al., 2018; Dong et al., 2017; Duan & Poon, 2014; Etxeberria et al., 2007; Fang et al., 2018; Fathifazl et al., 2011; Folino & Xargay, 2014; Gao & Zhang, 2018; Gómez-Soberón, 2002; Ibrahm & Abbas, 2017; Katkhuda & Shatarat, 2017; Kou et al., 2007, 2008; Liu et al., 2017; Meesala, 2019; Pedro et al., 2015; Pereira et al., 2012; Thomas et al., 2013, 2014; Wang et al., 2019; Yang et al., 2008; Younis & Pilakoutas, 2013; Zega & Di Maio, 2011; Zhang et al., 2014; 郭磊 et al., 2019); this was split into three phases: the training stage, representing 70% of the data (181 samples), validation stage, representing 15% of the data set (38 samples), and the testing stage, representing 15% of the data (38 samples) (Aghayari Hir et al., 2023; Benemaran, 2023). For this purpose, parameters such as water (W), cement (C), natural concrete aggregate content (NCA), recycled concrete aggregate content (RCA), Superplasticizer (SP), maximum aggregate size of RCA ($DMRAC$), density of RCA ($RORCA$), water absorption of RCA ($WRCA$), fibers (FV), fiber type (FT), 1-Steel fiber, 2-Carbon fiber, 3- Polypropylene fiber, 4-Basalt fiber, 5-Glass fiber, 6-Woolen fiber have been considered as input parameters to estimate the indirect tensile strength (STS) of recycled aggregate concretes.

The quantitative amounts of the input and output parameters are depicted in Table 1. To generate a precise STS, estimate for RCA, ten factors are included in models as inputs. Moreover, Fig. 1 showcases frequency diagrams illustrating the introduced attributes alongside their corresponding targets. It also visualizes input and output data distribution and examines any anomalies present. The Pearson correlation coefficient is a quantitative measure utilized to assess the degree of linear relationship between data points in a scatterplot. Its primary function is to gauge the association level between two distinct variables, with a scale ranging from -1 to +1. A positive value signifies a positive linear correlation, suggesting that an increase in one variable typically corresponds with a rise in the other. Conversely, a negative value showcases a negative linear correlation, implying that the other tends to diminish as one variable rises. Values closer to 0 suggest a weak or insignificant linear relationship; conversely, values nearer +1 or -1 signify a robust linear association between the variables. Fig. 2 illustrates the representation of the Pearson correlation coefficient.

Failure to appropriately consider the impact of significant positive or negative Pearson correlation coefficients on the outcomes may signal an ineffective methodology. Instances where variables exhibit poor correlation values should be acknowledged due to their significance. Therefore, incorporating these inputs in model development should yield the highest level of accuracy. As depicted in Fig. 2, the Pearson correlation coefficient (PCC) between RCA and NCA is -0.88, indicating a strong positive relationship. Additionally, the Pearson correlation coefficient (PCC) between $RORCA$ and WRCA is -0.56, representing the most negative correlation.

The core goals of sensitivity analysis in ML research encompass examining the effect of input variable modifications on outcomes, identifying key factors that affect model performance, boosting understanding of the model's behavior across diverse conditions, optimizing input variables for desired outcomes, and assisting in risk evaluation by pinpointing sensitive variables. Various open-source tools, including the Sensitivity Analysis Library ($SALib$), have been introduced to simplify the execution of sensitivity investigations (Iwanaga et al., 2022). SALib offers a range of techniques for conducting comprehensive sensitivity analysis, including Sobol, Morris, and $FAST$ methods. Decomposing the entire variance of the model output into discrete components linked to certain input variables is the fundamental idea underpinning $FAST$. This approach allows for identifying variables that significantly influence the model output and those with a lesser impact. In the context of the $FAST$ methodology, the indicators $S1$, ST, $S2$_conf, and ST _conf represent sensitivity-indices specific to this approach. The total-order sensitivity index for an input variable is defined by ST, which captures the variable's overall influence by considering its direct effect ($first-order$) and interactions with other factors. The ST value comprehensively assesses the variable's total impact on the outcome. The sensitivity analysis results for input parameters on the target variable, obtained through the $FAST$ method, are illustrated in Fig. 3, offering insights into the influence of each input characteristic. Among the attributes analyzed, the NCA and FT features exhibit the highest ST amounts of 0.993 and 0987, outperforming the RCA, FV, W, $RORCA$, SP, $DMRAC$, $WRCA$ and C of samples attributes, which recorded values of 0.974, 0.927, 0.91, 0.866, 0.838, 0.811, 0.722 and 0.591. This is seen as a favorable outcome, since it validates the physical correlation and predominant influence of aggregate composition and fiber type on the mechanical performance of reinforced concrete. These findings align with other experimental investigations that emphasize the significance of natural aggregate content and fiber reinforcement in enhancing crack resistance and tensile properties in concrete composites.

Table 1. The statistical explanation of the attributes considered

Phase	Index	Attributes										
		Inputs										Target
		W	C	NCA	RCA	SP	$DMRCA$	$RORCA$	$WRCA$	FV	FT	STS
		kg/m^3	kg/m^3	kg/m^3	kg/m^3	kg/m^3	mm	kg/m^3	%	%	$-$	MPa
Train	$Min.$	98.28	210	0	57	0	10	2010	1.9	0	0	1.38
	$Max.$	343.5	600	1143	1474	7.8	25	2640	10.9	7.7	6	7.61
	$St.D.$	37.601	60.996	365.744	392.130	1.626	4.151	159.257	1.845	0.955	1.782	1.078
	$Skew.$	1.294	0.360	0.540	0.176	1.581	-0.760	-0.795	1.088	5.703	0.843	1.015
	$Avg.$	184.964	371.746	328.168	757.802	1.063	18.367	2424.331	5.518	0.389	1.376	3.041
	$Kurt.$	5.793	1.189	-1.107	-0.971	2.087	-0.196	0.243	1.785	39.346	-0.932	1.771
Validation	$Min.$	98.28	158	0	59	0	10	2010	1.9	0	0	1.64
	$Max.$	343.5	514.5	1111	1474	3.5	25	2661	10.9	1.5	4	6.2
	$St.D.$	42.916	72.999	362.339	378.943	1.015	4.341	157.346	1.924	0.348	1.459	1.029
	$Skew.$	2.135	-0.398	-0.031	0.540	1.466	-0.762	-0.831	0.928	2.432	1.636	0.865
	$Avg.$	188.956	360.552	441.826	607.433	0.606	17.961	2435.421	5.186	0.163	0.763	3.056
	$Kurt.$	7.608	0.836	-1.424	-0.572	1.123	-0.256	0.774	2.630	6.222	1.202	0.780
Test	$Min.$	98.28	275	0	185	0	10	2010	2.25	0	0	1.43
	$Max.$	259	470.1	1132	1474	7.8	25	2640	10.9	5	5	7.02
	$St.D.$	28.743	52.110	333.697	340.756	2.135	4.506	137.273	1.664	0.882	1.805	1.161
	$Skew.$	-0.325	-0.549	0.391	0.521	1.888	-0.650	-0.958	1.315	3.856	0.960	1.027
	$Avg.$	185.455	370.447	326.705	739.217	1.192	17.000	2458.263	5.045	0.404	1.289	3.173
	$Kurt.$	1.633	-0.479	-1.006	-0.332	3.229	-1.125	1.453	3.234	19.286	-0.784	2.216

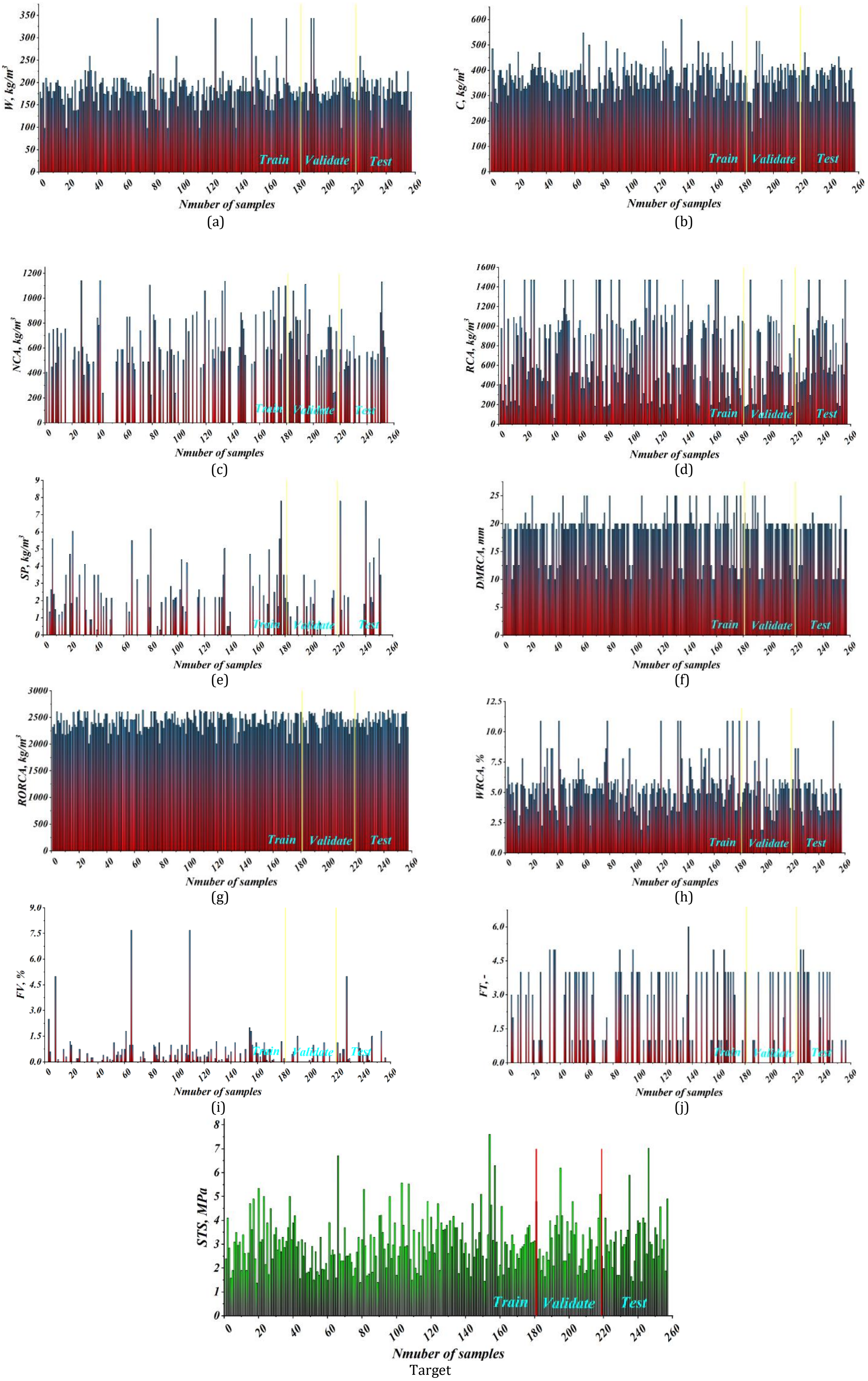

Fig. 1 The bar chart of the attributes in the train, validation, and test stages

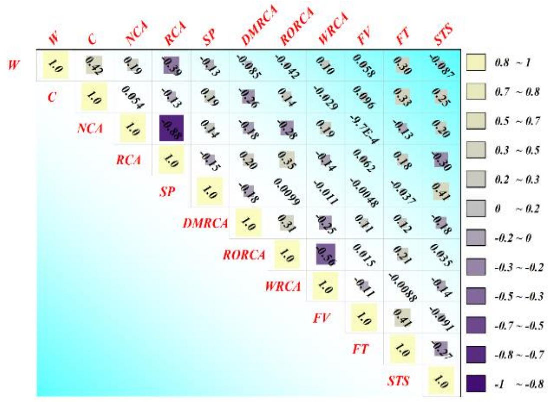

Fig. 2 The matrix visualization of Pearson correlation

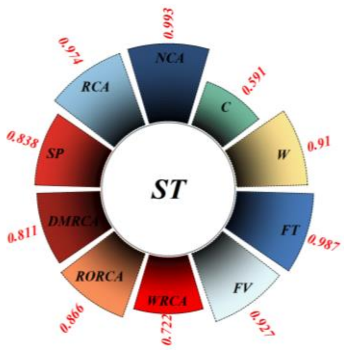

Fig. 3 Impact of attributes on the target (Sensitivity analysis)

3. Employed AI-Based Algorithms

3.1 Artificial Hummingbird Algorithm (ARHA)

In (Zhao et al., 2022), a novel bio-inspired improved algorithm called AHA was developed to address complex nonlinear optimization problems, particularly those involving high-dimensional search spaces, multimodal objective functions, and engineering design constraints. The expansion of the AHA algorithm aimed to replicate the remarkable flight abilities and clever searching strategies exhibited by hummingbirds in their everyday environment. The models replicate pivotal, diagonal, and in all directions, encompassing different flight abilities employed in diverse searching tactics. The search tactics encompass various approaches, such as guided searching, regional searching, and migrating searching. These tactics are employed, alongside creating a visiting table, to replicate hummingbirds' nourishment resource memory performance. The subsequent parts comprehensively describe the three primary models utilized in this algorithm. Fig. 4 demonstrates three flight treatments of hummingbirds.

Guided Searching

To enhance searching, this method incorporates three distinct flight conducts. These flights conduct, namely in all directions, diagonally, and pivotal flight are effectively simulated by introducing a direction switch vector (D) during searching. This vector, fully defined in Ref. (Zhao et al., 2022), accurately indicates if one or more directions are available in a d-dimensional area. Ultimately, the guided search conduct is numerically expressed as below:

$$v_i(t+1) = X_{ta}(t) + h.D.\left(X_i(t) - X_{ta}(t)\right) \quad (1)$$

The situation of the aim nourishment resource is denoted as $X_{ta}(t)$, while h represents the guiding agent that is generated based on the usual distribution and D is the direction matrix/vector that determines the direction of the factor's motion. $X_i(t)$ displays the situation of the ith nourishment resource at time t. Equation (1) describes the process of hummingbird-guided searching, incorporating different flight patterns. This equation enables each present nourishment resource to adjust its situation near the aim nourishment resource. The following formula determines the update of the ith nourishment resource's situation:

$$X_i(t+1) = \begin{cases} X_i(t) \;\; iff\left(X_i(t)\right) < f(v_i(t+1)) \\ v_i(t+1) \qquad\qquad otherwise \end{cases} \quad (2)$$

Regional Searching

Hummingbirds tend to explore novel nourishment resources after consuming the nectar from a specific flower rather than returning to previously visited resources. Consequently, these agile birds can easily venture to nearby situations within their territory, seeking alternative nourishment resources that may surpass their present one. The subsequent equation serves as a numerical representation of the regional searching tactic employed by hummingbirds to identify potential nourishment resources.

$$v_i(t+1) = X_i(t) + b.D.X_i(t) \quad (3)$$

The regional agent, represented by the variable b, is determined by the usual distribution. Equation (3) enables every hummingbird, irrespective of its situation, to efficiently and easily locate a fresh nourishment resource within its nearby area, considering its flight abilities. When the regional searching tactic is applied, updating the visit table regularly becomes essential.

Migration Searching

When nourishment availability diminishes within the vicinity regularly visited by a hummingbird, the hummingbird will generally relocate to a more distant nourishment resource. In the AHA algorithm, migration coefficient is designated to facilitate this movement. Suppose the number of repetitions surpasses the predetermined threshold of the migration coefficient. In that case, the hummingbird presently positioned at the nourishment resource with the lowest rate of nectar replenishment will relocate to a nourishment resource accidentally generated within the quest area. The visit table will display the revised data regarding the novel nourishment resource, as the hummingbird chooses to forsake its previous resource in favor of the fresh one. The transition of a hummingbird from a nectar resource with the slowest replenishment rate to a recently established resource can be determined accidentally by utilizing the subsequent relation:

$$X_{wor}(t+1) = \vec{lb} + \left(\vec{ub} - \vec{lb}\right).\vec{r} \quad (4)$$

$X_{wor}\ (t+1)$ is the fresh location of the worst resolution in the crowd at repetition $(t+1)$. The vector '$\vec{r}$ ' is accidentally assigned within the range of 0 and 1. The lowest border $(\vec{lb})$ and the highest border $(\vec{ub})$ define the limits for each dimension in the improved issue. The algorithm for AHA is outlined in Algorithm 1.

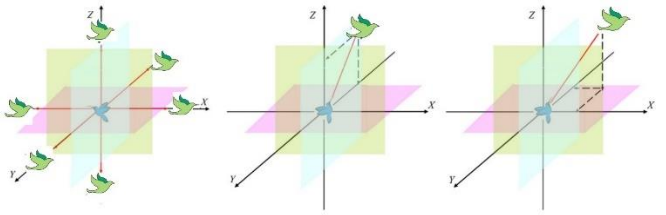

Fig. 4 Three flight treatments of hummingbirds (i) axial, (ii) diagonal, (iii) omnidirectional flight.

3.2 Chimp Optimization Algorithm (ChOA)

The ChOA, an improved algorithm inspired by the normal conduct of chimps, operates as a throng-based system and consists of four distinct stages: driving, chasing, blocking, and assaulting (Khishe & Mosavi, 2020). The initial stage of the ChOA procedure involves the accidental generation of chimpanzees. This is achieved by employing numerical methods to create groups and assigning chimpanzees accidentally to one or more of these four groups. Eqs. (5) and (6) illustrate the victim's inclination and endeavor in this context.

$$X_{chimp}(t+1) = X_{prey}(t) - 2fr_1 - f\left|2r_2X_{prey}(t) - m.X_{chimp}(t)\right| \quad (5)$$

$$m = Chaotic_{vector} \quad (6)$$

The value of repetitions is illustrated by t, the great solution gained so far is represented by X_{prey}, and the improved situation of the chimp is indicated by X_{chimp}. It is important to mention that the subordinate f undergoes a non-linear decline from 2.5 to 0. Additionally, the number of r_1 and r_2, which are accidentally set within the interval [0,1], contributes to the randomness of the algorithm. The Chaotic_vector is denoted by m (Saffari et al., 2022).

Without information about the initial victim situation, using a victim allows for the statistical replication of chimpanzee conduct. As stated in equations (7) and (8), ChOA will select and keep four of the most promising chimpanzees it has collected thus far. Meanwhile, other factors will be compelled to relocate based on the whereabouts of these top-performing chimpanzees (Khishe & Mosavi, 2020).

$$x(t+1) = \frac{1}{4} \times (x_1 + x_2 + x_3 + x_4) \quad (7)$$

Whereas

$$x_1 = x_{Attacker} + a_1 . |c_1 x_{Attacker} - m_1 x| \ , x_2 = x_{Barrier} - a_2 . |c_2 x_{Barrier} - m_2 x|$$

$$x_3 = x_{Chaser} + a_3 . |c_3 x_{Chaser} - m_3 x| \quad , \quad x_4 = x_{Driver} - a_4 . |c_4 x_{Driver} - m_4 x| \quad (8)$$

Eventually, the utilization of disorderly parameters is implemented to replicate the social incentive behavior of traditional ChOA, as demonstrated in Equation (9).

$$X_{chimp}(t+1) = \begin{cases} Eq. (5) & P_m < 0.5 \\ Chaotic_{vector} & P_m \geq 0.5 \end{cases} \quad (9)$$

The ChOA procedure stream illustrates the chimpanzees' conduct in response to an accidental quantity, denoted as P_m, within the interval (0,1]. In the presence of a quest area with D dimensions, the chimpanzees will strategically create hyperspheres surrounding the most improved situation discovered thus far. Fig. 5 depicts the location updating of chimps and the impacts of |a| on it.

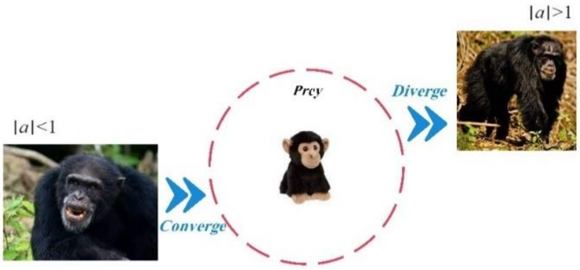

Fig. 5 Location updating of chimps and impacts of |a| on it

3.3 Random Forests Analysis (RFA):

The accidental forest algorithm utilizes both continuous and classified variables. Its underlying concept revolves around a collection of n decision trees. These decision trees consist of accidental variables $X_i = (X_1, \ldots X_P)^T$, representing input parameters, and accidental variables Y_i, representing result parameters (Kinga & Adam, 2015). The primary uncertainty lies in determining the probability distribution of the connections among the variables, denoted as $P_{XY}(X_i, Y_i)$.

In every node, the analyses are conducted using binary division. The initial node of the decision tree, referred to as the "root," encompasses data regarding all the input parameters. On the other hand, the non-split Nodes, known as ultimate nodes, are crucial in determining the decision tree's ultimate structure.

In situations with persistent issues, the division is established by determining a specific point of schism. It is assumed that quantities lower than this division point will progress towards the left descendant, while higher quantities will progress towards the proper descendant. Conversely, in classification issues, the forecasted variable is assigned an amount from a subset of classes denoted as $S = \{s_i, \ldots s_i\}$. The subsets representing the selected class expand in the left direction, while the remaining subsets expand in the right direction (Ghosh, 2009).

The partitioning of the offspring within a node occurs after evaluating all potential variable combinations and, subsequently, selecting the most suitable one based on a specified standard (Breiman, 2001).

The standard for regression issues is expressed below, as stated in (Breiman, 2001).

$$Q = \frac{1}{n} \sum_{i=1}^{n} (y_i - \bar{y})^2 \quad (10)$$

In the scenario where there is an issue involving K classes, the Gini indicator standard, which is derived from (Breiman, 2001), is utilized with y representing the arithmetic meaning of the variable under consideration in the node.

$$Q = \sum_{K \neq \acute{K}}^{K} \hat{P}_K \hat{P}_{\acute{K}} \quad (11)$$

The evaluations of $\hat{P}_K$ and $\hat{P}_{\acute{K}}$ are derived from the observations of classes k and K′ in the node, respectively. According to (Breiman, 2001), the evaluation of $\hat{P}_K$ is determined.

$$\hat{P}_K = \frac{1}{n} \sum_{i=1}^{n} I(y_i = k) \quad (12)$$

The divisions within the nodes continue until the algorithm's collection stop standard is satisfied, at which point the decision tree's result variable is revealed.

The primary objective of the accidental forest algorithm is to identify a suitable forecasting subordinate f (X) that can accurately predict the entire forest variable Y. This forecasting subordinate f is derived through the process of minimizing the loss subordinate $L(Y, f(X))$, which is established on the foundation of (Hastie et al., 2009).

$$E_{XY} \ L(Y, f(X)) \quad (13)$$

$L(Y, f(X))$represents the distance between $f(X)$ and Y, which serves as a potential solution for quadratic improved issues formulated using Eq. (16). This equation is derived from the work of [39].

$$L(Y, f(X)) = (Y - f(X))^2 \quad (14)$$

According to [65], it is anticipated that when assessing the lowest of $E_{XY} \left(L(Y, f(X)) \right)$,it signifies that:

$$f(x) = E(YIX = x) \quad (15)$$

The Bayes theorem [40] is well-known for regression issues and zero-one taxonomy duties, expressed as Eq. (16).

$$f(x) = argmax_{y \in Y} P(Y = yIX = x) \quad (16)$$

Consequently, by utilizing the data gathered from individual decision trees $h_1(x), \ldots, h_J(x)$, the value of the subordinate $f(x)$ can be determined, resulting in the overall outcome of the forest. In the case of regression duties, the subordinate $f(x)$calculates the average quantity (17) of the individual results obtained, as demonstrated in (Ghosh, 2009):

$$f(x) = \frac{1}{J} \sum_{j=1}^{J} h_j(x) \quad (17)$$

The prediction made by the jth tree for input x is $h_j(x)$. In taxonomy duties, the most commonly forecasted class (18) is denoted as $f(x)$, as mentioned in [34].

$$f(x) = argmax_{y \in Y} \sum_{j=1}^{J} I(y = h_j(x)) \quad (18)$$

3.4 Coupled RFA Models: RFAA, and RFAC

Optimizing the *RF*'s basic settings is critical to enhance the classification performance and obtain better findings for this investigation. The majority of the study focused on three crucial elements: $n_{estimators}$ (The number of decision trees), max_{depth} (The most significant amount of depth for decision trees), and $max_{features}$ (The highest number of features for DTs).

- $n_{estimators}$: A restricted number of estimators could result in an inadequately fitted estimate. The simulation may demonstrate a lack of complexity and may not accurately represent the underlying patterns in the data. Augmenting the quantity of estimators may bolster the model's resilience. However, there is a point at which adding more trees may not significantly improve speed and might instead increase computational costs.
- max_{depth}: A modest maximum depth constrains the complexity of individual trees. This could lead to underfitting, a situation in which the model cannot sufficiently capture complex patterns in the data. Trees with a higher maximum depth provide a more substantial capacity to capture complex patterns accurately. However, it also increases the probability of overfitting, in which the algorithm demonstrates excellent results on the training data but operates poorly on new, unfamiliar data.
- $max_{features}$: Using a few traits per split might lead to underfitting since the trees may not consider enough information to make accurate predictions. The presence of a high number of traits per split might result in overfitting since it can cause trees to become too specialized for the training data. This might lead to insufficient extrapolation of new data.

An outline of the processes that are used in the construction of *RF* is shown below:

- We cleaned the data, removed missing values, and eliminated outliers as necessary during the pre-processing stage.
- The data set was obtained systematically and divided into three sections, one part for analysis, one for validation, and the last part for testing, using the ratios suggested by the literature.
- Both algorithms' hyperparameters were initialized to values within predefined intervals before the first RF programs ran.
- It was achieved by using state-of-the-art optimization techniques (*ARHA* and CHOA) to identify the optimal values for the hyperparameters.
- The RF tests were trained using a unique dataset. The optimal hyperparameters were used throughout the validating and testing procedures, and further datasets were chosen to assess the variables.
- To evaluate the efficacy of the methodology, appropriate metrics are considered and calculated.

3.5 Metrics

To evaluate the performance of the developed *RF* Several metrics were considered and calculated. The equations are as follows: R^2, *RMSE*, normalized *RMSE*, *MSE*, Theil inequality error, index of agreement, performance index, and objective function.

$$R^2 = \left(\frac{\sum_{g=1}^{G} (n_g - \bar{n})(z_g - \bar{y})}{\sqrt{\left[\sum_{g=1}^{G} (n_g - n)^2\right]\left[\sum_{g=1}^{G} (y_g - \bar{y})^2\right]}} \right)^2 \quad (19)$$

$$RMSE = \sqrt{\frac{1}{G}\sum_{g=1}^{G}\left(y_g - n_g\right)^2} \quad (20)$$

$$NRMSE = RMSE/\bar{y} \quad (21)$$

$$MAE = \frac{1}{G}\sum_{g=1}^{G}\left|y_g - n_g\right| \quad (22)$$

$$TIC = \frac{\sqrt{\frac{1}{G}\sum_{g=1}^{G}(y_g - n_g)^2}}{\left(\sqrt{\frac{1}{G}\sum_{g=1}^{G}{y_g}^2} + \sqrt{\frac{1}{G}\sum_{g=1}^{G}{n_g}^2}\right)} \quad (23)$$

$$IA = 1 - \frac{\sum_{g=1}^{G}(n_g - y_g)^2}{\sum_{g=1}^{G}(|n_g - \bar{n}| + |y_g - \bar{n}|)^2} \quad (24)$$

$$PI = \frac{1}{\bar{n}}\frac{RMSE}{\sqrt{R^2+1}} \quad (25)$$

$$OBJ = \left(\frac{g}{G} \times \frac{RMSE+MAE}{R^2+1}\right)^{Train} + \left(\frac{g}{G} \times \frac{RMSE+MAE}{R^2+1}\right)^{Validate} + \left(\frac{g}{G} \times \frac{RMSE+MAE}{R^2+1}\right)^{Test} \quad (26)$$

The observed target, the mean of the observed target, the estimated target, and the mean of the estimated target are represented by the variables n_g, $\bar{n}$, y_g, and $\bar{y}$ in these equations, in that order. G indicates the count of rows of the database. g_{train}, $g_{validate}$ and g_{test} are the number of rows of datasets in the training, validating, and testing subsets, respectively.

4. Simulation Outcome

This research demonstrates the results of using the RF technique with the $CHOA$ and $ARHA$ methods to determine the STS of fiber reinforced RAC. Fig. 6 shows the measured and predicted amounts of STS throughout the learning, validation, and assessment stages of the $RF-CH$ and $RF-AR$ methods. Moreover, the chart shows the ratio of simulated to observed STS. The precision of the techniques for predicting STS was assessed using several indicators, including MAE, R^2, $NRMSE$, $RMSE$, TIC, SI, IA, PI, and OBJ. The rule of the optimization algorithms was to determine the optimal values of the hyperparameters, where the results are provided in Table 2. Table 3 depicts the assessments of the designs, emphasizing the optimal situation and the scores attained during the testing, validating, and training phases. In addition, the study compares its results with earlier research that used deep neural networks (DNN) (Alarfaj et al., 2024) and genetic programming (GEP) (Alabduljabbar et al., 2024) to confirm the developed models' dependability and assess the accuracy improvement.

The $RF-CH$ and $RF-AR$ methods show great potential for correctly forecasting the STS of fiber reinforced RAC, according to the results. The $RF-AR$ approach exhibited high reliability, with R^2 of 0.9942, 0.9824, and 0.9913 throughout the learning, validating, and assessment stages. $RF-AR$ had higher results than $RF-CH$, with R^2 values of 0.9796, 0.9566, and 0.9694, respectively. Improving the method's reliability might be achieved by including more error-based metrics. Smaller numbers suggest more efficacy for specific performance requirements. The $RF-AR$ criteria show much lower values than the $RF-CH$ criteria, with a variation of about 50% in the training, validating, and testing sections. The $RF-AR$ version had lower values of the stated metrics compared to the $RF-CH$ method, indicating the reliability of the framework in forecasting the STS of fiber reinforced RAC. For example, regarding the values of the TIC, $RF-AR$ depicted the lowest values at 0.0128, 0.0213, and 0.0171 wconcerning0.0241, 0.0333 and 0.0318 related to $RF-CH$ for the train, validation and test phases, in that order. The comprehensive metric included various metrics in one equation and data number of phases called OBJ were considered (The smaller, the better). The values obtained of this index depicted the accep, cap F minus cap C, and $RF-CH$ at 0.1332, with a reduction of almost 50%.

As can be displayed in Fig. 6b, the simulated STS per observed STS ratio is shown using the normal distribution technique. A smaller and more prominent distribution suggests a greater degree of dependability. This distribution makes it evident that throughout the training, validating, as well as testing stages, the $RF-AR$ outperformed the $RF-CH$. This manifests as more defined lower and upper bounds and a more prominent peak at one line.

The scholarly output generated by DNN (Alarfaj et al., 2024), and GEP (Alabduljabbar et al., 2024) has been employed to compare the findings of this study with a superior method ($RF-AR$). The scheme displayed greater accuracy in comparison to both DNN (Alarfaj et al., 2024), and GEP (Alabduljabbar et al.,2024), with $RF-AR$ values above those reported in the literature. The reported values of MAE, R^2, $RMSE$, and PI were compared with those of the $RF-AR$. Regarding DNN (Alarfaj et al., 2024), it was observed that great approvement of the R^2 and PI values. For example, the values of PI declined from 0.055 to 0.0136 (Train), and from 0.038 to 0.0183 (Test). Turning to the result of the GEP (Alabduljabbar et al.,2024), great improvements were observed considering the values of the $RMSE$, and MAE.

The $RF-AR$ strategy performed better, even if the $RF-CH$ method was dependable in forecasting the STS of fiber reinforced RAC, according to the previously stated reasoning and the data displayed in Table 3 and Fig. 6.

Table 2. The parameters of the created frameworks

Optimization and initial parameters					
$ARHA$	Iterations	200	$CHOA$	Iterations	200
	Population	40		Population	30
	Tries	10		Tries	10
	Migration coefficient	$2n$		r_1 and r_2	[0,1]
				m	Chaotic
Hyperparameters tunned RFs					
$RF-AR$	$n\_estimators$	36	$RF-CH$	$n\_estimators$	45
	max_depth	21		max_depth	18
	$max\_features$	41		$max\_features$	28

Table 3. The simulation outcomes and comparison with the literature

Metrics	Phase	Frameworks from this study		Frameworks from literature	
		$RF-CH$	$RF-AR$	DNN $(Alarfaj\ et\ al., 2024)$	GEP $(Alabduljabbar\ et\ al., 2024)$
R^2	Train	0.9796	0.9942	0.914	0.9604
	Validation	0.9566	0.9824		
	Test	0.9694	0.9913	0.94	0.9962
$RMSE$	Train	0.1551	0.0826		0.226
	Validation	0.215	0.1375		
	Test	0.2162	0.1157		0.16
$NRMSE$	Train	0.0513	0.0272		
	Validation	0.07	0.045		
	Test	0.0668	0.0361		
MAE	Train	0.079	0.0374		0.135
	Validation	0.1075	0.0528		
	Test	0.1235	0.048		0.12
TIC	Train	0.0241	0.0128		
	Validation	0.0333	0.0213		
	Test	0.0318	0.0171		
IA	Train	0.9947	0.9985		
	Validation	0.9886	0.9954		
	Test	0.9909	0.9975		
PI	Train	0.0256	0.0136	0.055	
	Validation	0.0356	0.0226		
	Test	0.0343	0.0183	0.038	
OBJ		0.1332	0.0687		

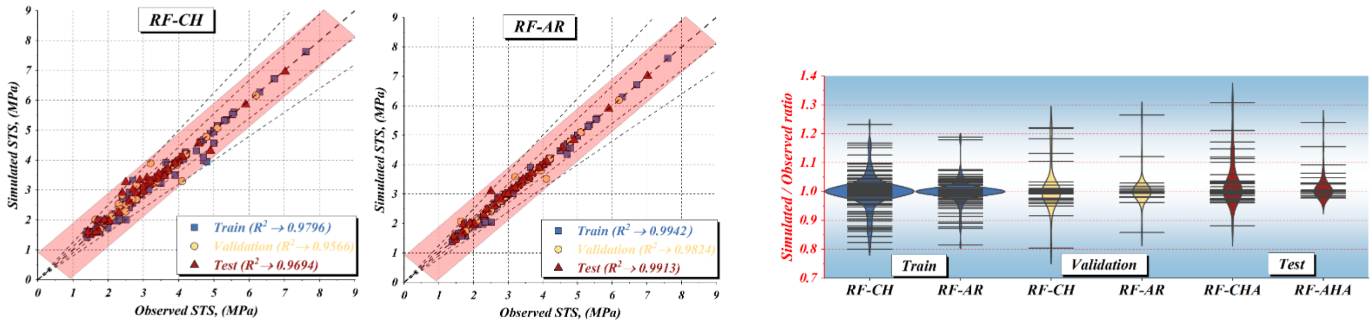

(a) Correlation (b) Variance ratio

Fig. 6 The visualization form of the simulation outcomes

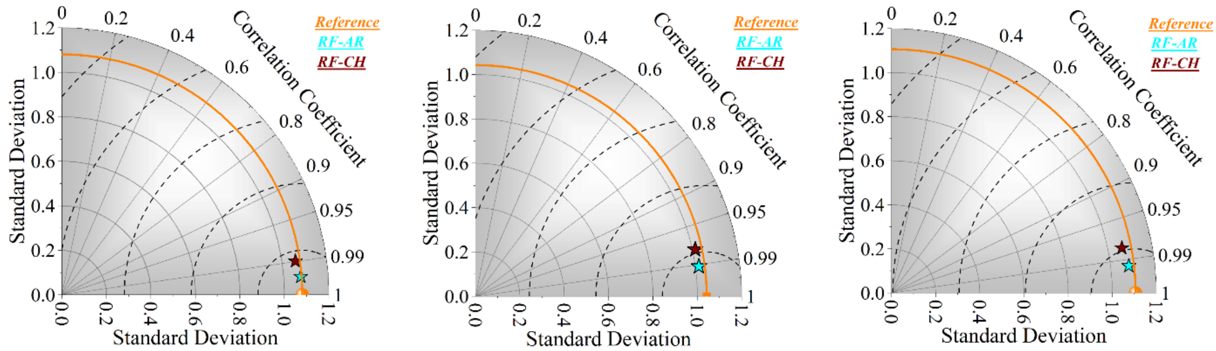

(a) Train (b) Validation (c) Test

Fig. 7 Performance of models using Taylor diagram

A Taylor diagram is an effective visual tool for assessing and comparing the performance of diverse schemes or simulations against observed data, utilizing three key statistical metrics: correlation coefficient, standard deviation, and root mean square error. In this diagram, the standard deviation is represented by the distance from the origin, indicating the variability of the model about the observed data. Values approaching 1 suggest a more substantial alignment between predictions and actual observations. The angle between the plotted points and the horizontal axis illustrates the correlation, while contours emanating from the origin signify models with lower errors. Points nearer the observation point, typically located along the x-axis, correspond to models exhibiting higher errors. This diagram effectively integrates these statistical measures into a single graphic, facilitating a straightforward comparison of model accuracy, variability, and correlation. The findings of this analysis are illustrated in Fig. 7, which presents the developed models during three training, validation, and testing steps. A model's proximity to the reference point indicates greater accuracy and acceptable reliability. Notably, in training and testing, the model identified as $RF-AR$ is positioned closer to the reference point than $RF-CH$ in all three steps, despite $RF-CH$ demonstrating higher accuracy.

The research recognizes a restriction in the applicability of the suggested models to real-world scenarios. Despite the models being meticulously trained, verified, and tested using literature-based data, their efficacy may not entirely translate to real-world situations, particularly when input variables surpass the original data range. To address this, the authors used a multi-phase assessment technique and several performance indicators, therefore augmenting model dependability. Nonetheless, further measures, such validation using external datasets or field testing, are advised to verify the models' relevance in actual building settings.

5. Conclusion

Machine learning algorithms are created in this work for the splitting tensile strength (STS) of fiber-reinforced recycled aggregate concrete (RAC). To do this, the potent random forests (RF) framework is taken into consideration. The RF framework uses the chimp optimization algorithm (CHOA) and artificial hummingbird optimization ($ARHA$) for hyperparameter tweaking and selecting the greatest performing combination of hyperparameters. A data set including 257 data points and 10 input variables was taken from peer-reviewed published research and arbitrarily split into three phases: testing, validating, and training. The study compares its results with earlier research that used deep neural networks *(DNN)* (Alarfaj et al., 2024) and genetic programming (GEP) (Alabduljabbar et al., 2024) to confirm the developed models' dependability and assess the accuracy improvement.

The $RF-CH$ and $RF-AR$ methods show great potential for properly forecasting the STS of fiber reinforced RAC, according to the results. The $RF-AR$ approach exhibited high reliability, with R^2 values of 0.9942, 0.9824, and 0.9913 throughout the learning, validating, and assessment stages. $RF-AR$ had higher results than $RF-CH$, with R^2 values of 0.9796, 0.9566, and 0.9694, respectively.

Regarding the error-based metrics, the $RF-AR$ criteria showed much lower values than the $RF-CH$ criteria, with a variation of about 50% in the training, validating, and testing sections. The $RF-AR$ version had lower values of the stated metrics compared to the $RF-CH$ method, indicating the reliability of the framework in forecasting the STS of fiber reinforced RAC.

Considering the values of the TIC, $RF-AR$ depicted the lowest values at 0.0128, 0.0213, and 0.0171 concerning 0.0241, 0.0333, and 0.0318 related to $RF-CH$ for the train, validation, and test phases, respectively.

The obtained values of OBJ index depicted the acceptability of the $RF-AR$ at 0.0687 concerning $RF-CH$ at 0.1332, with a reduction of almost 50%.

The scholarly output generated by DNN (Alarfaj et al., 2024), and GEP (Alabduljabbar et al.,2024) have been employed, to compare the findings of this study with a superior method ($RF-AR$). The framework demonstrated greater accuracy in comparison to both DNN (Alarfaj et al., 2024), and GEP (Alabduljabbar et al.,2024), with $RF-AR$ values above those reported in the literature.

The Taylor diagram effectively visualizes model performance by integrating key statistical metrics, allowing for easy comparison of accuracy and variability. While $RF-AR$ consistently positions closer to the reference point than $RF-CH$ across training, validation, and testing phases, $RF-CH$ still shows higher accuracy.

The $RF-AR$ strategy performed better, even if the $RF-CH$ method was dependable in forecasting the STS of fiber reinforced RAC, according to the previously stated reasoning and the data.

Authorship Contribution Statement

Chen Xi: Writing-Original draft preparation, Conceptualization, Supervision, Project administration.

Xiao Chen: Methodology, Software

Min Xiao: Formal analysis, Language review

Lang Wu: Validation

References

Afkhami Hoor, S., & Esmaeili-Falak, M. (2024). Innovative Approaches for Mitigating Soil Liquefaction: A State-of-the-Art Review of Techniques and Bibliometric Analysis. Indian Geotechnical Journal. https://doi.org/10.1007/s40098-024-01120-3

Aghayari Hir, M., Zaheri, M., & Rahimzadeh, N. (2023). Prediction of rural travel demand by spatial regression and artificial neural network methods (Tabriz County). Journal of Transportation Research (Tehran), 20(4), 367–386. https://doi.org/10.22034/tri.2022.312204.2970

Akça, K. R., Çakır, Ö., & İpek, M. (2015). Properties of polypropylene fiber reinforced concrete using recycled aggregates. Construction and Building Materials, 98, 620–630. http://dx.doi.org/10.1016/j.conbuildmat.2015.08.133

Alabduljabbar, H., Farooq, F., Alyami, M., & Hammad, A. W. A. (2024). Assessment of the split tensile strength of fiber reinforced recycled aggregate concrete using interpretable approaches with graphical user interface. Materials Today Communications, 38, 108009. http://dx.doi.org/10.1016/j.mtcomm.2023.108009

Alarfaj, M., Qureshi, H. J., Shahab, M. Z., Javed, M. F., Arifuzzaman, M., & Gamil, Y. (2024). Machine learning based prediction models for spilt tensile strength of fiber reinforced recycled aggregate concrete. Case Studies in Construction Materials, 20, e02836. https://doi.org/10.1016/j.cscm.2023.e02836

Ali, B., & Qureshi, L. A. (2019). Influence of glass fibers on mechanical and durability performance of concrete with recycled aggregates. Construction and Building Materials, 228, 116783. http://dx.doi.org/10.1016/j.conbuildmat.2019.116783

Ali, M. A. S., PP, F. R., & Salama Abd Elminaam, D. (2022). A feature selection based on improved artificial hummingbird algorithm using random opposition-based learning for solving waste classification problem. Mathematics, 10(15), 2675. http://dx.doi.org/10.3390/math10152675

Alnaggar, O., Jagadale, B. N., & Narayan, S. H. (2022). MRI brain tumor detection using boosted crossbred random forests and chimp optimization algorithm based convolutional neural networks. Int J Intell Eng Syst, 15(2), 36–46. http://dx.doi.org/10.22266/ijies2022.0430.04

Amin, M. N., Ahmad, A., Khan, K., Ahmad, W., Nazar, S., Faraz, M. I., & Alabdullah, A. A. (2022). Split tensile strength prediction of recycled aggregate-based sustainable concrete using artificial intelligence methods. Materials, 15(12), 4296. https://doi.org/10.3390/ma15124296

Andreu, G., & Miren, E. (2014). Experimental analysis of properties of high performance recycled aggregate concrete. Construction and Building Materials, 52, 227–235. http://dx.doi.org/10.1016/j.conbuildmat.2013.11.054

Babak, A., Shayan, R., P, S. M., Navid, C., S, F. A., & Mazdak, T. (2024). Cold-Formed Cross-Sectional Folds with Optimal Signature Curve. Journal of Engineering Mechanics, 150(8), 04024045. https://doi.org/10.1061/JENMDT.EMENG-7708

Bagherabad, M. B., Rivandi, E., & Mehr, M. J. (2025). Machine Learning for Analyzing Effects of Various Factors on Business Economic. Authorea Preprints. https://doi.org/10.36227/techrxiv.174429010.09842200/v1

Bayrami, B. (2021). Estimation of splitting tensile strength of modified recycled aggregate concrete using hybrid algorithms. Available at SSRN 3992623. https://doi.org/10.6180/jase.202412_27(12).0005

Benemaran, R. S. (2023). Application of extreme gradient boosting method for evaluating the properties of episodic failure of borehole breakout. Geoenergy Science and Engineering, 226, 211837. https://doi.org/10.1016/j.geoen.2023.211837

Benemaran, R. S., Esmaeili-Falak, M., & Kordlar, M. S. (2024). Improvement of recycled aggregate concrete using glass fiber and silica fume. Multiscale and Multidisciplinary Modeling, Experiments and Design, 7(3), 1895–1914. http://dx.doi.org/10.1007/s41939-023-00313-2

Breiman, L. (2001). Random forests Mach Learn 45 (1): 5–32. ed.

Butler, L., West, J. S., & Tighe, S. L. (2013). Effect of recycled concrete coarse aggregate from multiple sources on the hardened properties of concrete with equivalent compressive strength. Construction and Building Materials, 47, 1292–1301. http://dx.doi.org/10.1016/j.conbuildmat.2013.05.074

Chakradhara Rao, M., Bhattacharyya, S. K., & Barai, S. V. (2011). Influence of field recycled coarse aggregate on properties of concrete. Materials and Structures, 44, 205–220. http://dx.doi.org/10.1617/s11527-010-9620-x

Chen, S., Lu, P., Li, B., Wang, L., Guo, L., & Zhang, J. (2022). Influence and evaluation analysis of different fibers on the performance of recycled aggregate pervious concrete. J. Basic Sci. Eng, 30, 208–218. http://dx.doi.org/10.32604/jrm.2020.013415

Chen, Y., Hu, Y., & Hu, X. (2022). Quasi-brittle fracture analysis of large and small wedge splitting concrete specimens with size from 150 mm to 2 m and aggregates from 10 to 100 mm. Theoretical and Applied Fracture Mechanics, 121, 103474. http://dx.doi.org/10.1016/j.tafmec.2022.103474

Das, C. S., Dey, T., Dandapat, R., Mukharjee, B. B., & Kumar, J. (2018). Performance evaluation of polypropylene fibre reinforced recycled aggregate concrete. Construction and Building Materials, 189, 649–659. http://dx.doi.org/10.1016/j.conbuildmat.2018.09.036

Dawei, Y., Bing, Z., Bingbing, G., Xibo, G., & Razzaghzadeh,doi B. (2023). Predicting the CPT-based pile set-up parameters using HHO-RF and PSO-RF hybrid models. Structural Engineering and Mechanics, An Int'l Journal, 86(5), 673–686. http://dx.doi.org/10.12989/sem.2023.86.5.673

Dong, J. F., Wang, Q. Y., & Guan, Z. W. (2017). Material properties of basalt fibre reinforced concrete made with recycled earthquake waste. Construction and Building Materials, 130, 241–251. http://dx.doi.org/10.1016/j.conbuildmat.2016.08.118

Duan, Z. H., & Poon, C. S. (2014). Properties of recycled aggregate concrete are made with recycled aggregates with different amounts of old adhered mortars. Materials & Design, 58, 19–29. http://dx.doi.org/10.1016/j.matdes.2014.01.044

Esmaeili-Falak, M., & Benemaran, R. S. (2023). Ensemble deep learning-based models to predict the resilient modulus of modified base materials subjected to wet-dry cycles. Geomechanics and Engineering, 32(6), 583. http://dx.doi.org/10.12989/gae.2023.32.6.583

Esmaeili-Falak, M., & Benemaran, R. S. (2024). Ensemble Extreme Gradient Boosting based models to predict the bearing capacity of micropile group. Applied Ocean Research, 151, 104149. https://doi.org/10.1016/j.apor.2024.104149

Esmaeili-Falak, M., Katebi, H., Vadiati, M., & Adamowski, J. (2019). Predicting triaxial compressive strength and Young's modulus of frozen sand using artificial intelligence methods. Journal of Cold Regions Engineering, 33(3), 04019007. http://dx.doi.org/10.1061/(ASCE)CR.1943-5495.0000188

Esmaeili-Falak, M., & Sarkhani Benemaran, R. (2024). Application of optimization-based regression analysis for evaluation of frost durability of recycled aggregate concrete. Structural Concrete, 25(1), 716–737. http://dx.doi.org/10.1002/suco.202300566

Etxeberria, M., Marí, A. R., & Vázquez, E. (2007). Recycled aggregate concrete as structural material. Materials and Structures, 40, 529–541. http://dx.doi.org/10.1617/s11527-006-9161-5

Fang, S.-E., Hong, H.-S., & Zhang, P.-H. (2018). Mechanical property tests and strength formulas of basalt fiber reinforced recycled aggregate concrete. Materials, 11(10), 1851. http://dx.doi.org/10.3390/ma11101851

Fathifazl, G., Razaqpur, A. G., Isgor, O. B., Abbas, A., Fournier, B., & Foo, S. (2011). Creep and drying shrinkage characteristics of concrete produced with coarse recycled concrete aggregate. Cement and Concrete Composites, 33(10), 1026–1037. http://dx.doi.org/10.1016/j.cemconcomp.2011.08.004

Folino, P., & Xargay, H. (2014). Recycled aggregate concrete–Mechanical behavior under uniaxial and triaxial compression. Construction and Building Materials, 56, 21–31. http://dx.doi.org/10.1016/j.conbuildmat.2014.01.073

Fonseca, N., De Brito, J., & Evangelista, L. (2011). The influence of curing conditions on the mechanical performance of concrete made with recycled concrete waste. Cement and Concrete Composites, 33(6), 637–643. http://dx.doi.org/10.1016/j.cemconcomp.2011.04.002

Gao, D., & Zhang, L. (2018). Flexural performance and evaluation method of steel fiber reinforced recycled coarse aggregate concrete. Construction and Building Materials, 159, 126–136. http://dx.doi.org/10.1016/j.conbuildmat.2017.10.073

Ghosh, D. (2009). Modern Multivariate Statistical Techniques: Regression, Classification, and Manifold Learning by IZENMAN, AJ. Oxford University Press. https://doi.org/10.1111/j.1541-0420.2009.01315_2.x

Gómez-Soberón, J. M. V. (2002). Porosity of recycled concrete with substitution of recycled concrete aggregate: An experimental study. Cement and Concrete Research, 32(8), 1301–1311. http://dx.doi.org/10.1016/S0008-8846(02)00795-0

Hassankhani, E., & Esmaeili-Falak, M. (2024). Soil–Structure Interaction for Buried Conduits Influenced by the Coupled Effect of the Protective Layer and Trench Installation. Journal of Pipeline Systems Engineering and Practice, 15(2), 04024012. http://dx.doi.org/10.1061/JPSEA2.PSENG-1547

Hastie, T., Tibshirani, R., Friedman, J. H., & Friedman, J. H. (2009). The elements of statistical learning: data mining, inference, and prediction (Vol. 2). Springer. http://dx.doi.org/10.1007/BF02985802

Hu, X., Li, Q., Wu, Z., & Yang, S. (2022). Modelling fracture process zone width and length for quasi-brittle fracture of rock, concrete and ceramics. Engineering Fracture Mechanics, 259, 108158. http://dx.doi.org/10.1016/j.engfracmech.2021.108158

Ibrahm, H. A., & Abbas, B. J. (2017). Mechanical behavior of recycled self-compacting concrete reinforced with polypropylene fibres. Journal of Architectural Engineering Technology, 6(2), 1–7. http://dx.doi.org/10.4172/2168-9717.1000207

Iwanaga, T., Usher, W., & Herman, J. (2022). Toward SALib 2.0: Advancing the accessibility and interpretability of global sensitivity analyses. Socio-Environmental Systems Modelling, 4, 18155. http://dx.doi.org/10.18174/sesmo.18155

Katkhuda, H., & Shatarat, N. (2017). Improving the mechanical properties of recycled concrete aggregate using chopped basalt fibers and acid treatment. Construction and Building Materials, 140, 328–335. http://dx.doi.org/10.1016/j.conbuildmat.2017.02.128

Khishe, M., & Mosavi, M. R. (2020). Chimp optimization algorithm. Expert Systems with Applications, 149, 113338. http://dx.doi.org/10.1016/j.eswa.2020.113338

Kinga, D., & Adam, J. B. (2015). A method for stochastic optimization. International Conference on Learning Representations (ICLR), 5, 6. https://doi.org/10.48550/arXiv.1412.6980

Kou, S. C., Poon, C. S., & Chan, D. (2007). Influence of fly ash as cement replacement on the properties of recycled aggregate concrete. Journal of Materials in Civil Engineering, 19(9), 709–717. http://dx.doi.org/10.1061/(ASCE)0899-1561(2007)19:9(709)

Kou, S. C., Poon, C. S., & Chan, D. (2008). Influence of fly ash as a cement addition on the hardened properties of recycled aggregate concrete. Materials and Structures, 41, 1191–1201. http://dx.doi.org/10.1617/s11527-007-9317-y

Kuijpers, M. (2020). Concrete is one of the most polluting materials in the world. Here's how we can make it sustainable. The Correspondent. September 9, 2020.

Kumarawadu, H., Weerasinghe, P., & Perera, J. S. (2024). Evaluating the Performance of Ensemble Machine Learning Algorithms over Traditional Machine Learning Algorithms for Predicting Fire Resistance in FRP Strengthened Concrete Beams. Electronic Journal of Structural Engineering, 24(3), 47–53. http://dx.doi.org/10.56748/ejse.24661

Liang, R., & Bayrami, B. (2023). Estimation of frost durability of recycled aggregate concrete by hybridized Random Forests algorithms. Steel and Composite Structures, 49(1), 91–107. https://doi.org/10.12989/scs.2023.49.1.091

Liu, H., Yang, J., Kong, X., & Xue, X. (2017). Basic mechanical properties of basalt fiber reinforced recycled aggregate concrete. The Open Civil Engineering Journal, 11(1). http://dx.doi.org/10.2174/1874149501711010043

Meesala, C. R. (2019). Influence of different types of fiber on the properties of recycled aggregate concrete. Structural Concrete, 20(5), 1656–1669. http://dx.doi.org/10.1002/suco.201900052

Mohammadi Yaychi, B., & Esmaeili-Falak, M. (2024). Estimating Axial Bearing Capacity of Driven Piles Using Tuned Random Forest Frameworks. Geotechnical and Geological Engineering. http://dx.doi.org/10.1007/s10706-024-02952-9

Moradi, G., Hassankhani, E., & Halabian, A. M. (2022). Experimental and numerical analyses of buried box culverts in trenches using geofoam. Proceedings of the Institution of Civil Engineers-Geotechnical Engineering, 175(3), 311–322. http://dx.doi.org/10.1680/jgeen.19.00288

Neshatfar, S., Magner, A., & Sekeh, S. Y. (2023). Promise and Limitations of Supervised Optimal Transport-Based Graph Summarization via Information Theoretic Measures. IEEE Access, 11, 87533–87542. https://doi.org/10.1109/ACCESS.2023.3302830

Neshatfar, S., & Sekeh, S. Y. (2024). Robust Subgraph Learning by Monitoring Early Training Representations. ArXiv Preprint ArXiv:2403.09901. https://doi.org/10.48550/arXiv.2403.09901

Pan, X., Xiao, Y., Suhail, S. A., Ahmad, W., Murali, G., Salmi, A., & Mohamed, A. (2022). Use of artificial intelligence methods for predicting the strength of recycled aggregate concrete and the influence of raw ingredients. Materials, 15(12), 4194. http://dx.doi.org/10.3390/ma15124194

Pedro, D., De Brito, J., & Evangelista, L. (2015). Performance of concrete made with aggregates recycled from precasting industry waste: influence of the crushing process. Materials and Structures, 48, 3965–3978. http://dx.doi.org/10.1617/s11527-014-0456-7

Pereira, P., Evangelista, L., & De Brito, J. (2012). The effect of superplasticizers on the mechanical performance of concrete made with fine recycled concrete aggregates. Cement and Concrete Composites, 34(9), 1044–1052. http://dx.doi.org/10.1016/j.cemconcomp.2012.06.009

Rivandi, E., & Jamili Oskouie, R. (2024). A Novel Approach for Developing Intrusion Detection Systems in Mobile Social Networks. Available at SSRN 5174811. http://dx.doi.org/10.2139/ssrn.5174811

Saffari, A., Zahiri, S. H., Khishe, M., & Mosavi, S. M. (2022). Design of a fuzzy model of control parameters of chimp algorithm optimization for automatic sonar targets recognition. Iranian Journal of Marine Technology, 9(1), 1–14. http://dx.doi.org/10.1080/0952813X.2021.1960639

Sun, X., Gao, Z., Cao, P., Zhou, C., Ling, Y., Wang, X., Zhao, Y., & Diao, M. (2019). Fracture performance and numerical simulation of basalt fiber concrete using three-point bending test on notched beam. Construction and Building Materials, 225, 788–800. http://dx.doi.org/10.1016/j.conbuildmat.2019.07.244

Thomas, C., Setién, J., Polanco, Ja., Alaejos, P., & De Juan, M. S. (2013). Durability of recycled aggregate concrete. Construction and Building Materials, 40, 1054–1065. http://dx.doi.org/10.1016/j.conbuildmat.2012.11.106

Thomas, C., Sosa, I., Setién, J., Polanco, J. A., & Cimentada, A. I. (2014). Evaluation of the fatigue behavior of recycled aggregate concrete. Journal of Cleaner Production, 65, 397–405. http://dx.doi.org/10.1016/j.jclepro.2013.09.036

Umba, L. N., Amir, I. Y., Gelete, G., Gökçekuş, H., & Uwanuakwa, I. D. (2024). Artificial hummingbird algorithm-optimized boosted tree for improved rainfall-runoff modelling. Journal of Hydroinformatics, 26(1), 203–213. http://dx.doi.org/10.2166/hydro.2023.187

Wang, Y., Hughes, P., Niu, H., & Fan, Y. (2019). A new method to improve the properties of recycled aggregate concrete: Composite addition of basalt fiber and nano-silica. Journal of Cleaner Production, 236, 117602. http://dx.doi.org/10.1016/j.jclepro.2019.07.077

Yang, K.-H., Chung, H.-S., & Ashour, A. (2008). Influence of Type and Replacement Level of Recycled Aggregates on Concrete Properties.

Younis, K. H., & Pilakoutas, K. (2013). Strength prediction model and methods for improving recycled aggregate concrete. Construction and Building Materials, 49, 688–701. http://dx.doi.org/10.1016/j.conbuildmat.2013.09.003

Yuan, F., Cheng, L., Shao, X., Dong, Z., Zhang, L., Wu, G., & He, X. (2020). Full-field measurement and fracture and fatigue characterizations of asphalt concrete based on the SCB test and stereo-DIC. Engineering Fracture Mechanics, 235, 107127. http://dx.doi.org/10.1016/j.engfracmech.2020.107127

Zarei, M., Mohseni, F., & Sohrabi, P. (2024). Correlates of spatial structure variability in Bushehr port-city: A comprehensive analysis using fuzzy cognitive mapping methodology. J. Infrastruct. Policy Dev, 8, 8789. http://dx.doi.org/10.24294/jipd.v8i11.8789

Zega, C. J., & Di Maio, A. A. (2011). Recycled concrete is made with waste ready-mix concrete as coarse aggregate. Journal of Materials in Civil Engineering, 23(3), 281–286. http://dx.doi.org/10.1061/(ASCE)MT.1943-5533.0000165

Zhang, X. B., Kuang, C. G., Fang, Z., Liu, X. H., Wang, G. Q., & Lai, S. (2014). Orthogonal experimental study on strength of steel fiber reinforced fly ash recycled concrete. J. Build. Mater, 17, 677–684. http://dx.doi.org/10.3969/j.issn.1007-9629.2014.04.021

Zhao, W., Wang, L., & Mirjalili, S. (2022). Artificial hummingbird algorithm: A new bio-inspired optimizer with its engineering applications. Computer Methods in Applied Mechanics and Engineering, 388, 114194. http://dx.doi.org/10.1016/j.cma.2021.114194

郭磊, 刘思源, 陈守开, 汪伦焰, & 薛志龙. (2019). 纤维改性再生骨料透水混凝土力学性能透水性和耐磨性研究. Transactions of the Chinese Society of Agricultural Engineering, 35(2). https://dx.doi.org/10.11975/j.issn.1002-6819.2019.02.020

Disclaimer

The statements, opinions and data contained in all publications are solely those of the individual author(s) and contributor(s) and not of EJSEI and/or the editor(s). EJSEI and/or the editor(s) disclaim responsibility for any injury to people or property resulting from any ideas, methods, instructions or products referred to in the content.